Silicon (2022) 14:5513–5526
https://doi.org/10.1007/s12633-021-01336-5

ORIGINAL PAPER

Quad-Band Circularly Polarized Tunable Graphene Based Dielectric Resonator Antenna for Terahertz Applications

P. Upender[1] · Amarjit Kumar[1]

Received: 9 June 2021 / Accepted: 17 August 2021 / Published online: 25 August 2021

Abstract
A Cylindrical Dielectric Resonator antenna (CDRA) along with silicon based Rectangular Dielectric Resonator (RDR) slab is proposed in this paper for terahertz (THz) applications. This antenna provides multi-band response at different resonant frequencies. Unique feature of the proposed antenna is, it provides Circular Polarization (CP) behaviour at quad band in the field of THz dielectric resonator antennas and also CP tuning is achieved by varying graphene potential of the antenna. Furthermore this antenna shows both Right Hand CP (RHCP) and Left Hand CP (LHCP) behaviour at different resonant frequencies. A rectangular slab is incorporated with CDRA knows CPDRA to achieve CP response. Results show that a maximum gain of 6.67 dB, maximum radiation efficiency of 89%, 10 dB Impedance Bandwidth (IBW) of 4.66% (8.59-9THz), 2.98% (10.88–11.21THz), 4.83% (14.19–13.52THz) and 5.86% (15.88–16.84), Axial Ratio Bandwidth (ARBW) of 1.83% (8.66–8.82 THz), 2.16% (10.94–11.18), 3.84% (13.26–13.78 THz) and 4.8% (16.04–16.83 THz) is achieved by the combination of CDRA and Rectangular slab. For antenna tunability, the upper layer of CDRA is layered with graphene material and CP performance of antenna is analyzed for different values of graphene chemical potential. This new approach for the tuning and obtained results make the proposed Quad band CP DRA as unique and is suitable for THz applications.

Keywords Circular polarization · Dielectric resonator antenna · Multi-band · Impedance bandwidth · Polarization

1 Introduction

DRA is first coined by Robert Richtmyer in the year 1939 and the first design and testing was carried out by Long et al. [1] in the year 1982 by considering for dielectric surface as a leaky waveguide model. Antenna is always a powerful and supreme part of wireless communication system [2, 3]. Over the past few decades, the design of DRA has caught many researchers attention because of its high RE, low loss, easy to excite, and wide IBW compared with micro strip antennas. Moreover, using the dielectric constant (ε) of the DRA material, size and bandwidth can be easily controlled to achieve high gain and high radiation efficiency [4–7]. For the next generation communication system, terahertz (THz) frequency has become a choice because of the crowded spectrum of microwave and mm wave [8–10]. Furthermore because of its high data rate and high bandwidth, enforces the researches to work in THz region. Many systems in present days provide single band, wide band or ultra wide band response in the microwave or mm wave region [8, 10–14]. Also considerable research is being made in the THz frequency region which provides multi band response [15–19]. Additionally, many approaches on the design of DRA is done in the THz range with different feed mechanisms [20–25]. Besides this, a common characteristic in any antenna which is preferred is CP behavior at different frequencies. In the case of LP antennas, multipath fading is quite severe. Polarization mismatch losses owing to transmitter and receiver misalignment are also a constraint of LP antennas. The usage of CP antennas completely eliminates these constraints. Recently in THz frequency region, DRA is implemented with CP radiation behavior [26–29].

Many current designs provide wide band, dual band, and single band responses, and very little research is done on antennas that provide resonance in multiple bands while also providing circular polarization characteristics in multiple

✉ P. Upender
pu721063@student.nitw.ac.in

Amarjit Kumar
amarjitk@nitw.ac.in

[1] Department of Electronics and Communication, National Institute of Technology, Warangal, Telangana, India

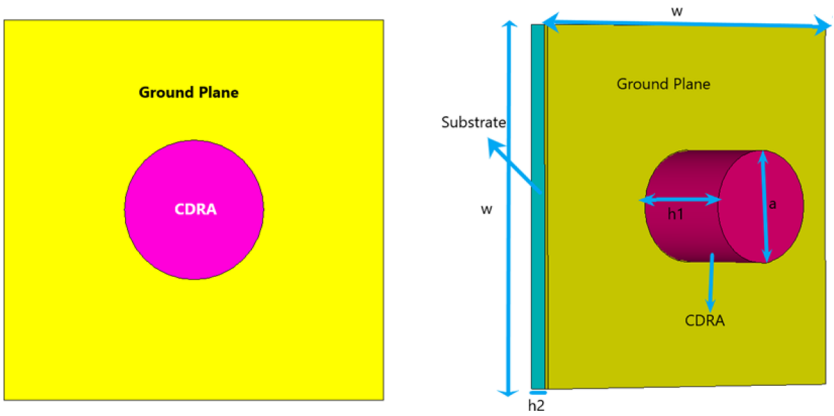

Fig. 1 CDRA **a** Top view **b** Side view (with dimension)

bands at THz frequencies. Another difficult task is getting high gain and high radiation efficiency at THz frequency. Apart from these issues, achieving tunability for multiband antennas is also an difficult task at THz frequency. For this, Graphene based antennas, could bring new capabilities to RF devices with its tunability behavior at THz frequency range. Graphene, in both single and multi-forms, has a number of specific characteristics, including high electrical conductivity and extreme thermal conductivity, making it ideal for RF antenna construction [30–32]. The antennas reported in [29, 33–39], are focused on multiband THz frequency based on graphene. These antennas reported less gain and less radiation efficiency.

To address all of these challenges, it is urgently needed to design an antenna that can give multiband response with high gain and high efficiency while tuning the resonance frequency and also CP tuning. In this paper a Circularly Polarized Dielectric Resonator antenna (CPDRA) is designed with high gain and high radiation efficiency. CDRA combined with rectangular slab known as CPDRA is implemented for terahertz (THz) applications to provide circular polarization. Unique feature of the proposed antenna is, it provides CP behaviour at quad band in the field of THz dielectric resonator antennas and also CP tunability is achieved by varying graphene potential. Proposed antenna shows both RHCP and LHCP behaviour at different resonant frequencies. Unlike other antennas which are discussed above, this antenna provides multi-mode circular polarization response at different resonant frequencies. The proposed CPDRA provides good impedance bandwidth (IBW) and ARBW. The parametric analysis on physical parameters of the antenna is carried out to analyze the performance of the antenna. For antenna frequency response tunability, the upper layer of CDRA is layered with graphene material with different values of chemical potential of the antenna. The proposed antenna has excellent gain, efficiency, and provides resonance in multi bands, as well as CP tuning is achieved at multiple resonant frequencies in the field of multiband THz DRAs.

This paper is arranged as follows: In section two different structures of antenna with CDRA is shown along with parametric analysis on different parameters. In section 3, the proposed model CPDRA for quad band CP response is discussed. Behaviour of proposed antenna with addition of graphene is discussed in section four and conclusion in section 5.

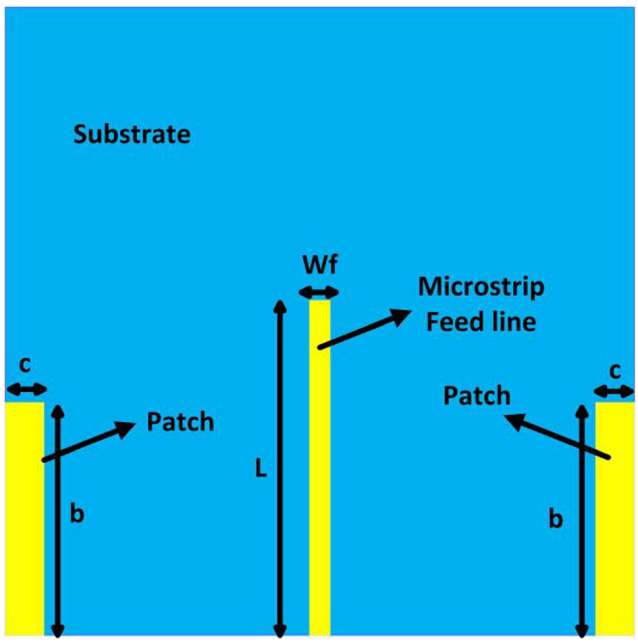

Fig. 2 Bottom view of the proposed DRA

Table 1 Dimensions of parameters (μm)

w	*h2*	*g*	*rout*	*rin*	*c*	*l*	*wf*	*a*	*h1*	*hr*	*wr*	*lr*
22	1.27	0.3	2	0.7	3	13.4	1	3.4	6.9	6	5	22

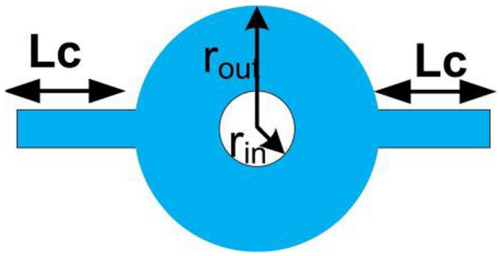

Fig. 3 Proposed Aperture slot configuration

2 Antenna Modelling, Operating Mechanism and Design Methodology

Figure 1 depicts the configuration CDRA. It consists of silicon CDRA (ε_r=11.9, μ_r=1, electric conductivity (σ) = 0.00025 S/m at T = 300 k) with aperture slot feed on the ground plane which is made up of copper. Silicon dioxide (SiO_2) material with dimensions of w × w × h_2, ε_r=3.9, μ_r=1 and loss tangent of 0.001 is used as dielectric substrate. The feed line is etched below the substrate up to the aperture slot.

Figure 1b shows dimensions of CDRA, bottom substrate and ground plane. The copper feed line etched on the bottom of the substrate having length l and width W_f as shown in Fig. 2. All the optimized dimensions (μm) are given in Table 1.

As depicted in Fig. 2 two patches are etched on the either side of substrate to direct the beam in a particular direction so that the directivity of antenna is enhanced. Electromagnetic waves can be prevented from radiating under the dielectric substrate by placing two symmetrical tiny metal sheets to the rear of the substrate. The dimension of patch is given by b × c to reduce spurious radiation under dielectric substrate [40]. The thickness of feed line is chosen so that the waves must be adequately concentrated on the surface. Coupling to the radiator must be accomplished by the proper choice of micro strip feed line (50 Ω) dimension at THz frequency range. To achieve the multi-band response the dimensions are calculated for getting resonance at terahertz frequency and then optimized for obtaining desired response. Simulation is carried out in CST Microwave Studio. The circular slot ring which is made on the ground plane is used for coupling efficient power to the DRA is depicted in Fig. 3.

In CDRA basically three modes will excite: Hybrid (HE and EH or HEM) mode, TE and TM modes. Hybrid modes will depend on azimuth angle (ϕ), whereas TE and TM modes will not depend on azimuth angle. CDRA basically excites HEM, $HEM_{npm+\delta}$, $EH_{npm+\delta}$, $EH_{0pm+\delta}$ and $TM_{0pm+\delta}$ where δ will range from 0 to 1. The resonant frequency of the $HEM_{11\delta}$ mode supported by a CDRA can be calculated using the following Eq. (1) [41].

$$f_{r(HEM11\delta)} = \frac{c}{2\pi r_d} \times \frac{6.324}{\sqrt{\varepsilon_{rd}+2}} \times \left[0.27 + 0.36\left(\frac{r}{2h_d}\right) + 0.02\left(\frac{r}{2h_d}\right)^2\right] \quad (1)$$

Where r is the radius and h_d is the height of CDRA.

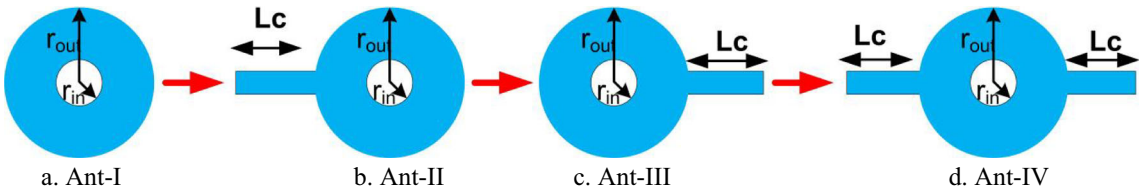

Fig. 4 Antenna configuration evolution. **a** circular slot without any arm **b** Circular slot with left side arm **c** Circular slot with right side arm. **d** Circular slot with two arms

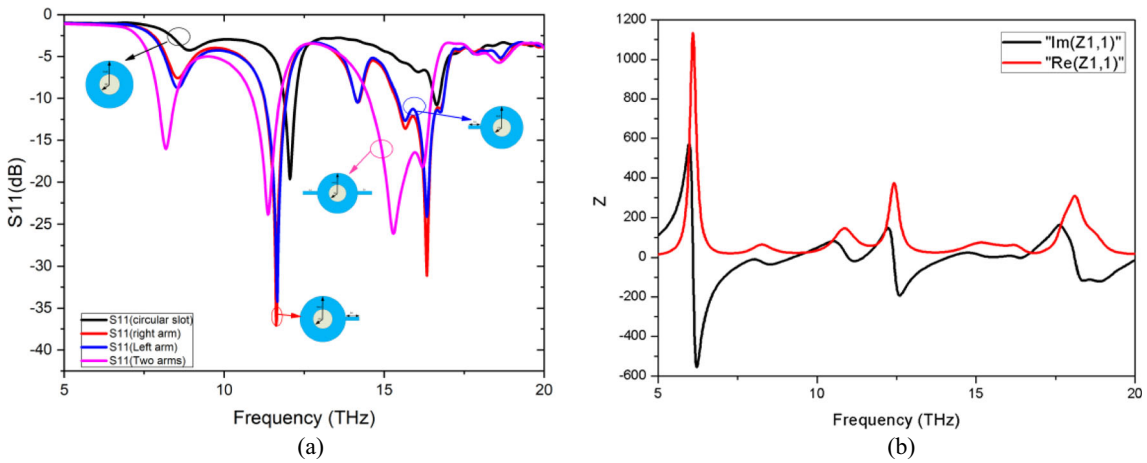

Fig. 5 **a** Frequency response (S_{11}) of CDRA **b** Impedance response

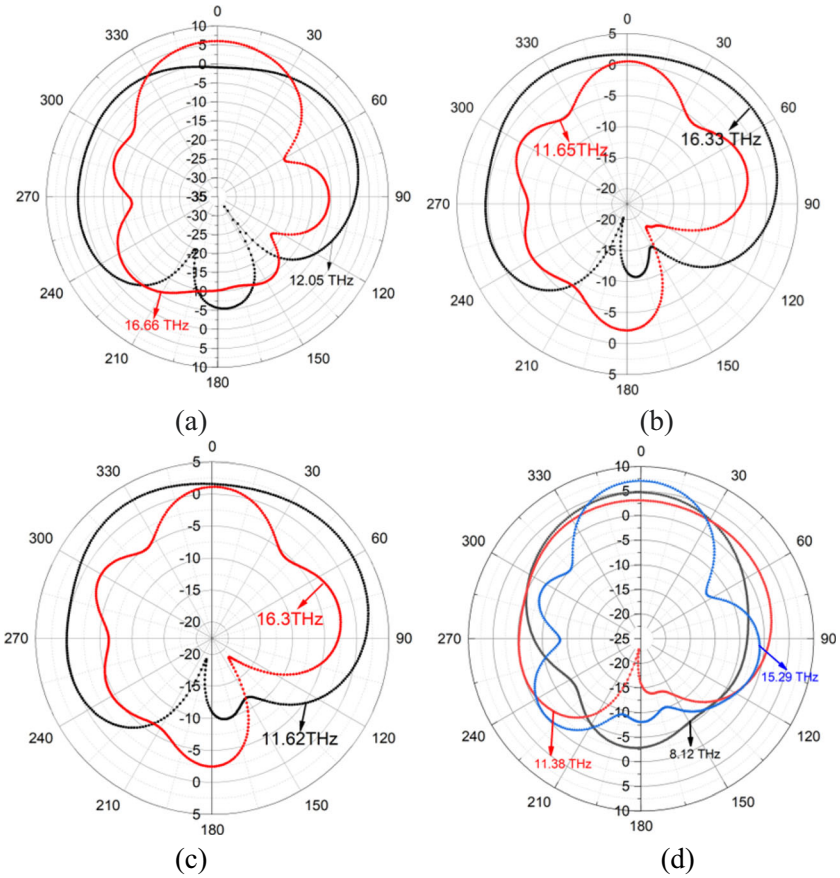

Fig. 6 2D radiation patterns for **a** Ant-I, **b** Ant-II, **c** Ant-III and **d** Ant-IV

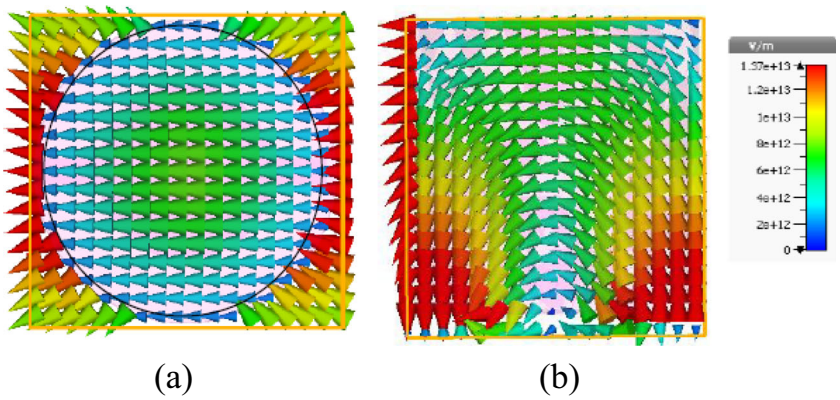

Fig. 7 E-Field distribution on CDRA at 8.12 THz **a** Top view (XY-Plane) and **b** Side view (XZ-Plane)

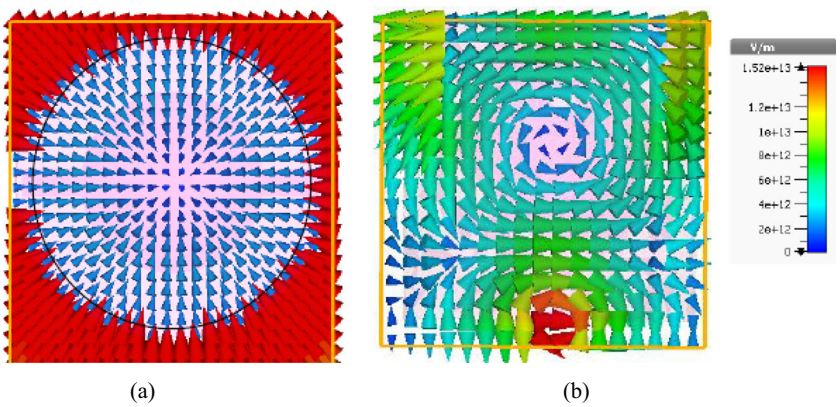

Fig. 8 E-Field distribution on CDRA at 11.38 THz **a** Top view (XY-Plane) and **b** Side view (XZ-Plane)

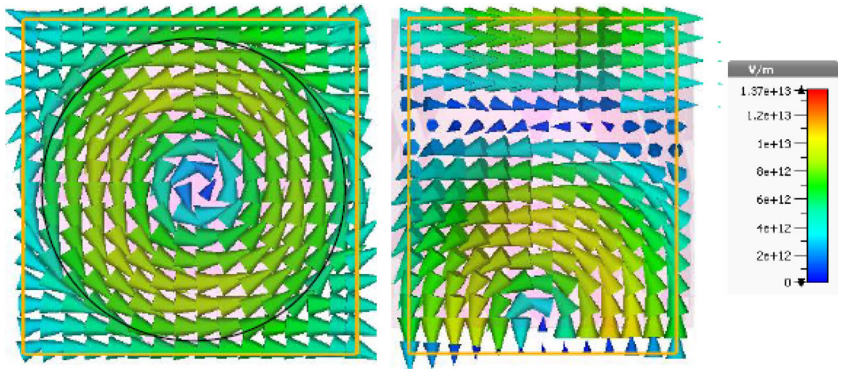

(a) (b)

Fig. 9 E-Field distribution on CDRA at 15.29 THz **a** Top view (XY-Plane), **b** Side view (XY-Plane)

2.1 Operating Mechanism of CDRA

In this section, the operating mechanism of the proposed CDRA is investigated. In order to commend the design analysis for multi band, CDRA without rectangular slab is used as the allusion antenna for investigation. Different slots are used to excite DRA to demonstrate the impact of feeding slot. The two arms on the either side of the circular slot feed are of length lc = 1.4 μm each (Fig. 3).

As depicted in Fig. 4, antenna -I is circular slot feed without any arm and is fed with micro strip feed which is etched at the bottom of the substrate. Figure 4b–d depicts left side arm with circular slot feed, right side arm with circular slot feed and circular slot with two arms having length ls. As depicted in Fig. 5, two resonant modes are excited when antenna is fed with circular slot (Ant-I) i.e., at 12.05THz and 16.66THz with an impedance bandwidth of 2.98% (11.87–12.23THz) and 0.9% (16.56–16.71THz) respectively. These frequencies are chosen based on the reflection coefficients (S_{11}). At these frequencies S_{11} is minimum (i.e., <-10 dB). At 12.056THz,

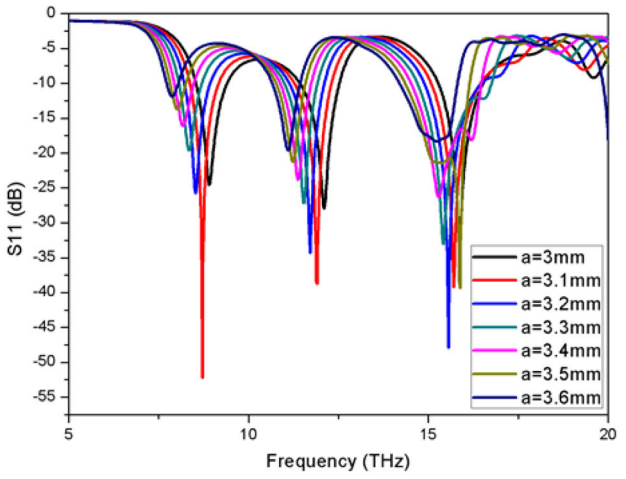

(a)

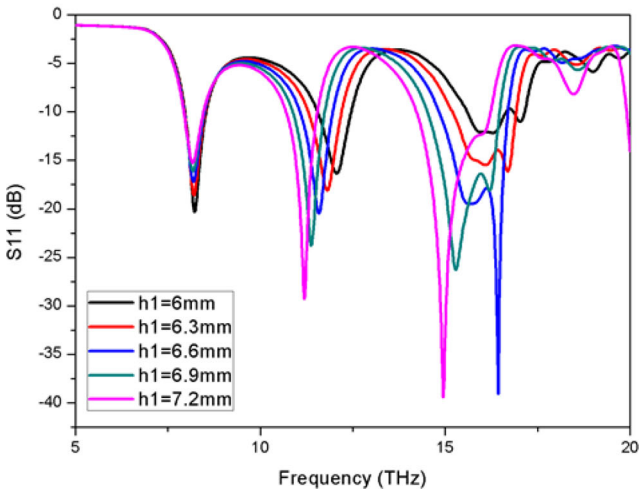

(b)

Fig. 10 Plot of frequency response for the CDRA with change in a. radius of CDRA and b. Height of CDRA h1

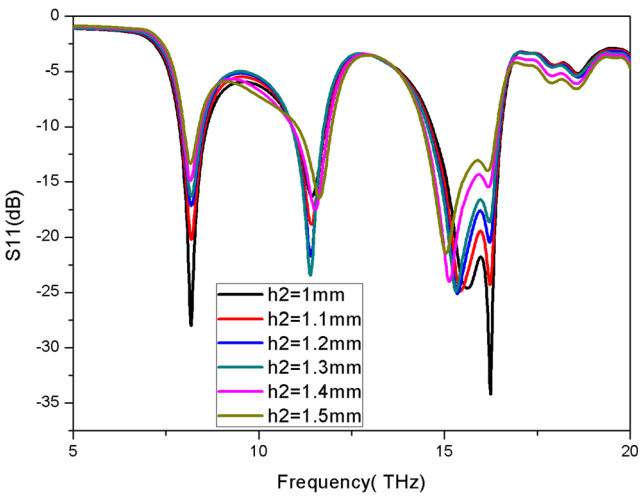

Fig. 11 Plot of frequency response for the CDRA with change in h2

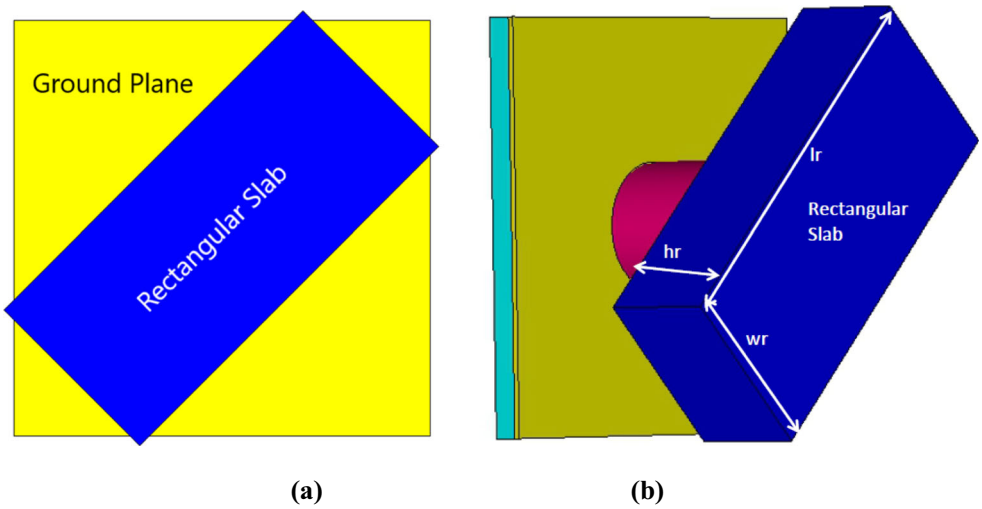

Fig. 12 Rectangular Slab on top of CDRA (CPDRA) **a** Top view **b** Side view (with dimensions)

S_{11} is approximately −19.5 dB and at 16.66THz, S_{11} is approximately −10.74 dB. Similarly when DRA is excited with Fig. 4b, it excites at two resonant frequencies at 11.65 and 16.33 THz with S_{11} of −34.2 dB at 11.65THz and − 23.9 dB at 16.33THz with impedance bandwidth of 5.86% 11.26–11.94 THz) and 8.98% (15.42–16.87 THz). When DRA is excited with Fig. 4c, it excites at two resonant frequencies at 11.62 (S_{11}= − 37.05 dB) and 16.33 THz (S_{11}= − 30.9) with impedance bandwidth of 5.87% (11.24–11.92 THz) and 9.3% (15.36–16.86 THz). Finally, the circular slot with two arms excites at three resonant frequencies as depicted in Fig. 5. One at 8.12THz with S_{11} of −16.04 dB, another one at 11.38THz with S_{11} of −23.8 dB and third one at 15.29THz with S_{11} of -26 dB. The impedance bandwidth in percentage is given by 6.7% (7.93–8.48 THz), 7.6% (11.74–10.87 THz) and 12.65% (14.51–16.47 THz). It can be observed that, considerable increase in impedance bandwidth with the proposed feed slot design (Ant-IV of Fig. 4). It is found that there is a shift in the resonant frequency from model a to d of antenna configuration as depicted in Fig. 5. Figure 1b confirms the generation of three modes of CDRA with ant-IV configuration.

Figure 6 shows the plot of radiation pattern for Ant-I, II, III and IV configurations. It is observed from the Fig. 6a that a gain of 3.6 and 6 dB is achieved at main lobe direction of 59° and 0° at resonant frequencies of 12.05 and 16.66 THz. A gain of 2.9 and 0.55 dB is achieved at main lobe direction of 55° and 1° at resonant frequencies of 11.65 and 16.33 THz as depicted in Fig. 6b. It is observed from the Fig. 6c that a gain of 2.8 and 1.1 dB is achieved at main lobe direction of 58° and 1° at resonant frequencies of 11.62 and 16.3 THz. A gain of 4.73, 3.15 and 7.08 dB is achieved at main lobe direction of 4°, 11° and 0° at resonant frequencies of 8.12, 11.38 and 15.29 THz as depicted in Fig. 6d. It is clear that maximum gain is achieved for the proposed slot (Ant-IV) compared to Ant-I, II and III.

Modes in CDRA can be identified based on the electric and magnetic field (E and H) distribution on CDRA. Figure 7 shows E-field and H-field distribution at 8.12 THz. It can be observed that $HEM_{11\delta}$ mode is propagating inside CDRA at 8.12 THz [41]. From Fig. 8, from the observation it is found that the resonant mode is similar to $TM_{01\delta}$ is excited at 11.38 THz. Similarly at third resonant frequency at 15.29 THz it is observed that $TE_{01\delta}$ mode is excited (Fig. 9).

2.2 Parametric Analysis

To analyze the performance of the antenna, the physical parameters are changed by keeping other parameters untouched. Height of the substrate h_2, height of CDRA h_1, and radius a CDRA (a) are the key parameters of the proposed antenna. Figure 10a depicts the frequency response of the proposed CDRA with change in radius (a)

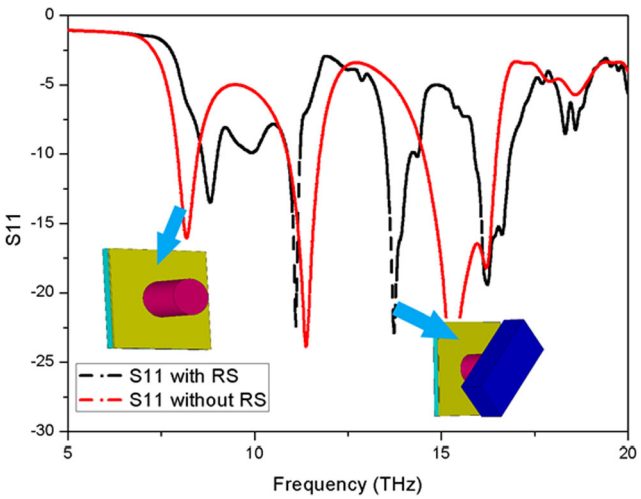

Fig. 13 Frequency response comparison between CDRA with rectangular slab (Black line) and without rectangular slab (Red line)

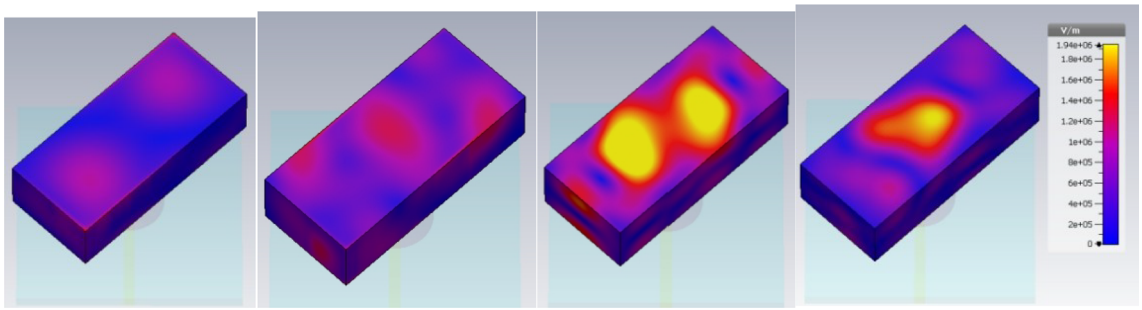

Fig. 14 Electric field distribution on isolated rectangular slab ((XY-Plane) along with amplitude level bar at **a** 8.79, **b** 11.1 **c** 13.7 **d** 16.2 THz

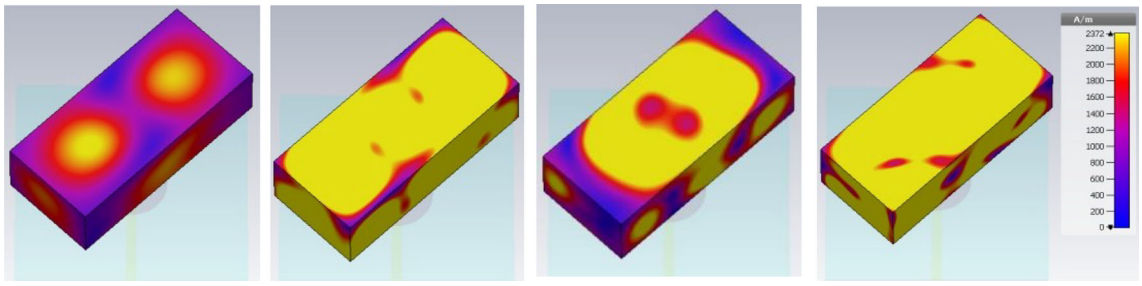

Fig. 15 Magnetic field distribution on isolated rectangular slab (XY-Plane) along with amplitude level bar at **a** 8.79, **b** 11.1 **c** 13.7 **d** 16.2 THz

of CDRA. It is noted that a good performance and good impedance matching is obtained with change in the radius of CDRA. However the number of resonant frequencies remain unchanged. Figure 10b depicts the frequency response with change in the height of CDRA (h1).

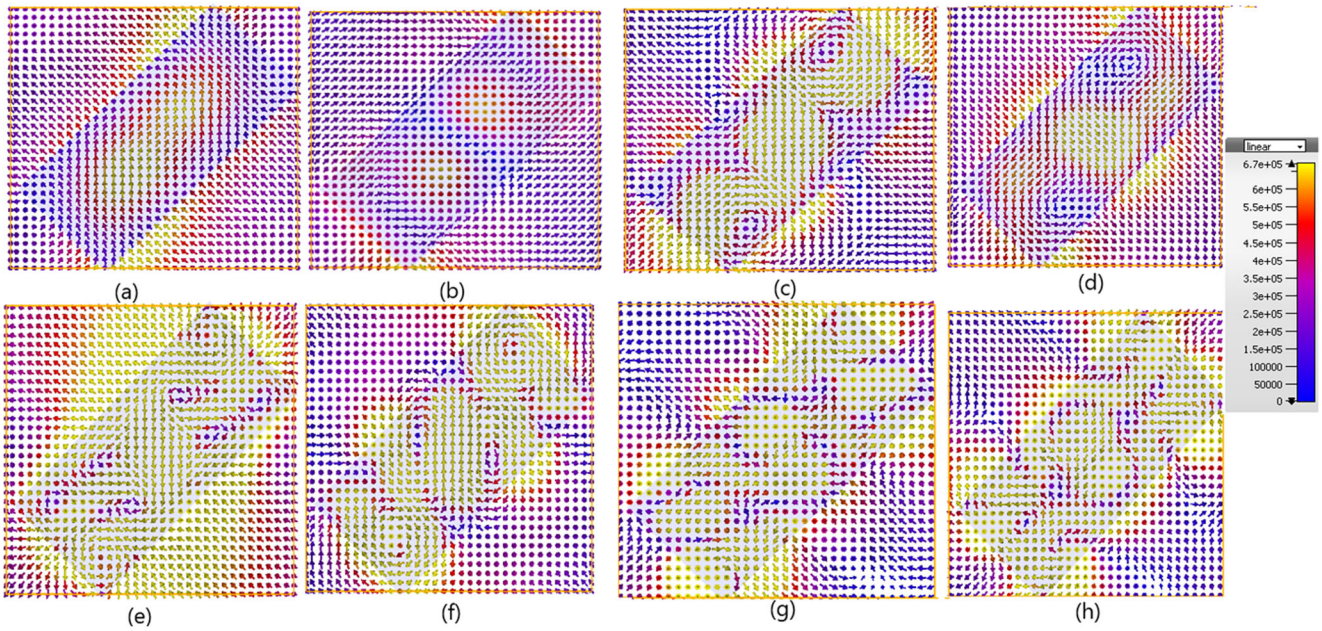

Fig. 16 Electric field vector distribution on rectangular slab (XY-Plane) at frequency of 8.79 THz **a** t = 0 and **b** t = T/4, at 11.1 THz **c** t = 0 and **d** t = T/4, at 13.7 THz **e** t = 0 and **f** t = T/4 and at 16.2 THz **g** t = 0 and **h** t = T/4

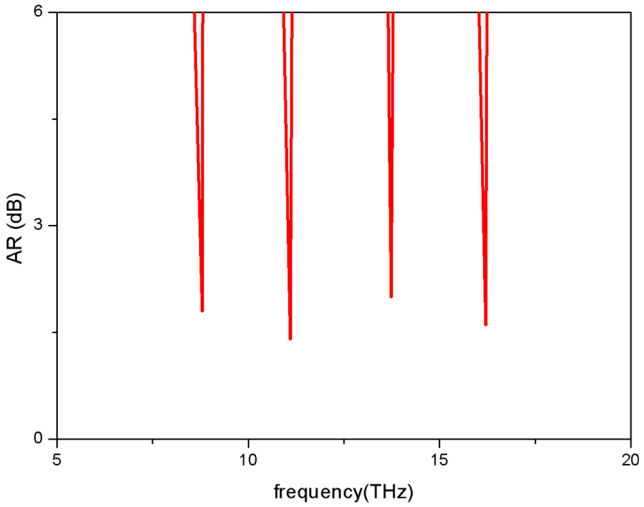

Fig. 17 Axial Ratio (AR) dB vs frequency plot for Rectangular slab along with CDRA

It is clear that when the height of CDRA is increases, better impedance matching is observed. In Fig. 11, the frequency response of antenna for change in substrate (SiO_2) thickness (h2) is investigated. From the above analysis it is clear that, CDRA resonates at three resonant frequencies and good impedance matching is observed even for the change of physical parameters. All these parameters are optimized and are depicted in Table 1.

3 Combination of Rectangular Dielectric Resonator Slab (RS) and CDRA

In order to achieve circular polarization, silicon based Rectangular dielectric slab inclined with 45° in clock wise direction is placed on top of CDRA as depicted in Fig. 12 with dimensions (μm) lr × wr × hr (22 × 5 × 6). As depicted in the plot of frequency response (Fig. 13) it can be observed that this combination of CDRA and Rectangular slab knows as Circularly Polarized Dielectric Resonator Antenna (CPDRA) provides resonance at four frequencies i.e., 8.79, 11.10, 13.73, 16.21 THz with 10 dB IBW of 4.66% (8.59-9THz), 2.98% (10.88–11.21THz), 4.83% (14.19–13.52THz) and 5.86%(15.88–16.84). The shift of resonant frequency between CDRA and CPDRA is due to the height of silicon based rectangular slab. The

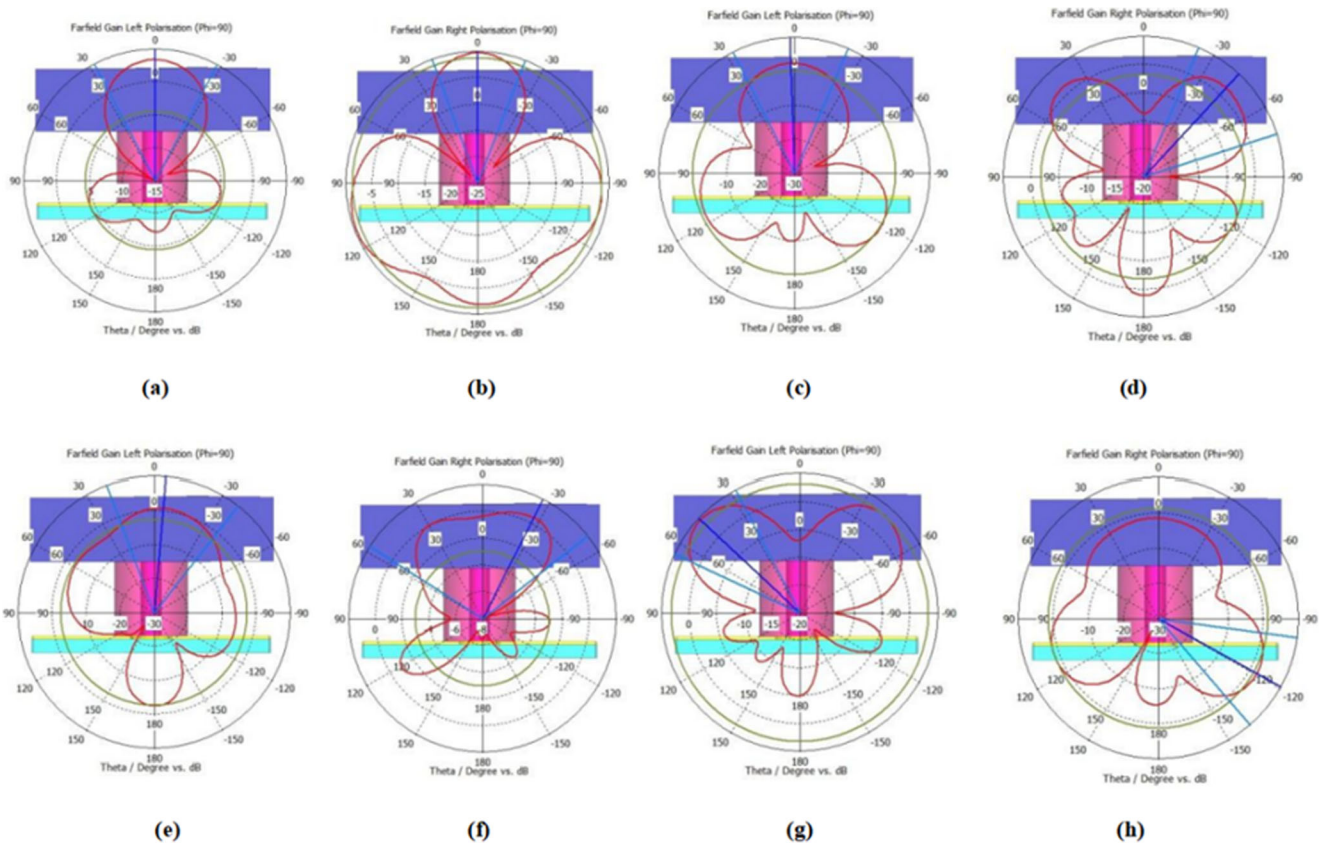

Fig. 18 Far field 2D radiation pattern for θ = 0° and φ = 90° at 8.79 **a** LHCP **b** RHCP, at 11.1 **c** LHCP **d** RHCP, at 13.7 **e** LHCP **f** RHCP at 16.2 THz **g** LHCP, **h** RHCP

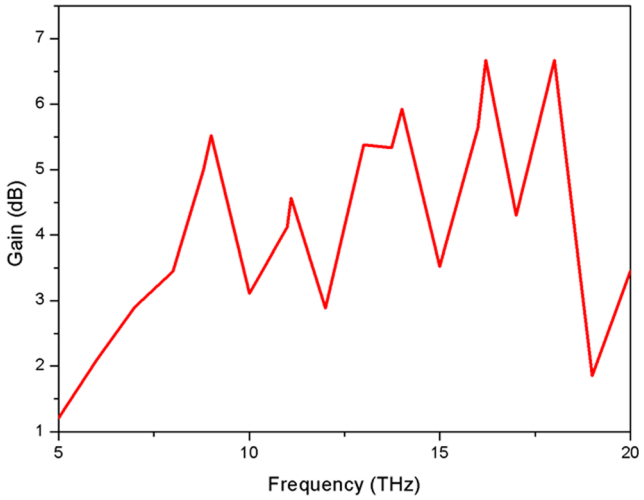

Fig. 19 Gain (dB) vs frequency plot

variation of EF and MF distribution at resonant frequencies on the top of Rectangular slab is shown in Figs. 14 and 15.

3.1 Mechanism of Circular Polarization

CP waves are generally excited by two orthogonal linearly polarized components with equal magnitude and with 90^0 phase between them. To analyze the behavior of CP, consider Fig. 16 which shows EF vector behavior (at f = 8.79, 11.1, 13.7 and 16.2 THz) at different time instants (t = 0, T/4). It can be observed that two orthogonal EFs are generated with equal magnitude at the resonant frequencies. From t = 0 to t = T/4 (Fig. 16a, b) at frequency of 8.79 THz, electric field vectors (EFV) are rotated by clock wise direction. This proves that Left Hand CP (LHCP) is generated. The arrangement of rectangular slab with 45^0 orientation leads to circular polarization. The generation of LHCP field can be observed at each time-quarter with 90^0 rotations of EF vectors. This rotation occurs due to the generation of higher order orthogonal degenerate modes. The field distribution is modified after placing rectangular slab. From this it is clear that addition of rectangular slab spun by 45^0 provides orthogonal degenerate modes which are expected and also required for CP response. Similarly at frequency of 11.1 THz (Fig. 16c, d)), it can be observed that EFV are rotated in anti-clock wise direction which means at this frequency the proposed DRA generates Right Hand CP (RHCP) wave. Similarly at frequencies of 13.7 and 16.2THz (Fig. 16e–h) it can be understood from the observation that LHCP wave is generated at both the frequencies. From this it is concluded that the proposed antenna generates quad band CP response at four resonant frequencies. This unique feature of the antenna makes it suitable for THz applications.

In order to elucidate the radiation characteristics effectively, plot of axial ratio (AR) and Polarization (LHCP and RHCP) are shown in Figs. 17 and 18. It is observed that proposed CPDRA produces CP characteristics as depicted in Fig. 17. A 3 dB ARBW of 1.83% (8.66–8.82 THz), 2.16% (10.94–11.18), 3.84% (13.26–13.78 THz) and 4.8% (16.04–16.83 THz) is depicted in Fig. 17 which means the proposed antenna produces quad band CP response at four bands. Figure 18 shows the LHCP and RHCP far-field radiation pattern components for four resonant frequencies i.e., at 8.79, 11.1, 13.73 and 16.2 THz. The antenna provides the dominant LHCP field at resonant frequency of 8.79, 13.73 and 16.2 THz, whereas at frequency of 11.1 THz, RHCP wave dominates. Figure 19 exhibits the plot between Gain (dB) vs frequency. This antenna provides a gain of 5 dB, 4.5 dB, 5.5 dB and 6.67 dB at four resonant frequencies i.e., 8.79, 11.10, 13.73, 16.21 THz.

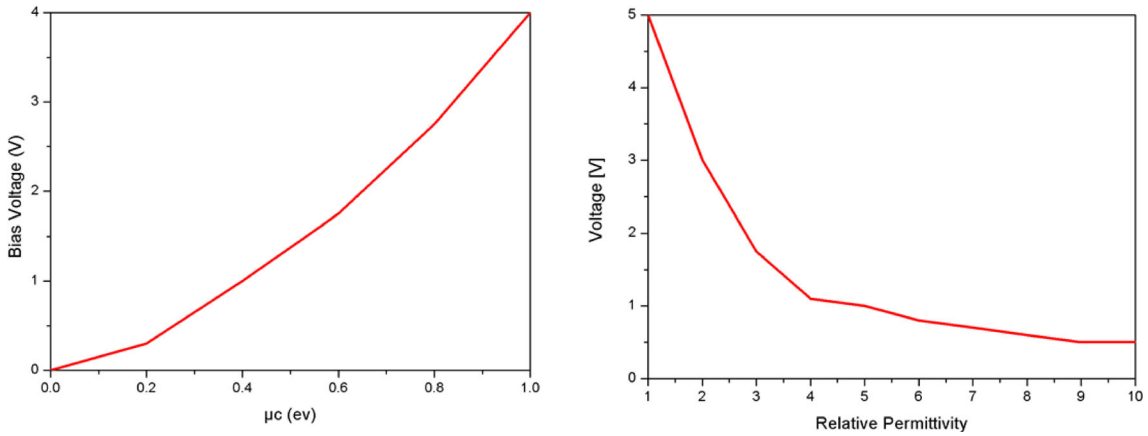

(a) (b)

Fig. 20 **a** μ_c vs Bias voltage **b** Relative Permittivity vs Voltage

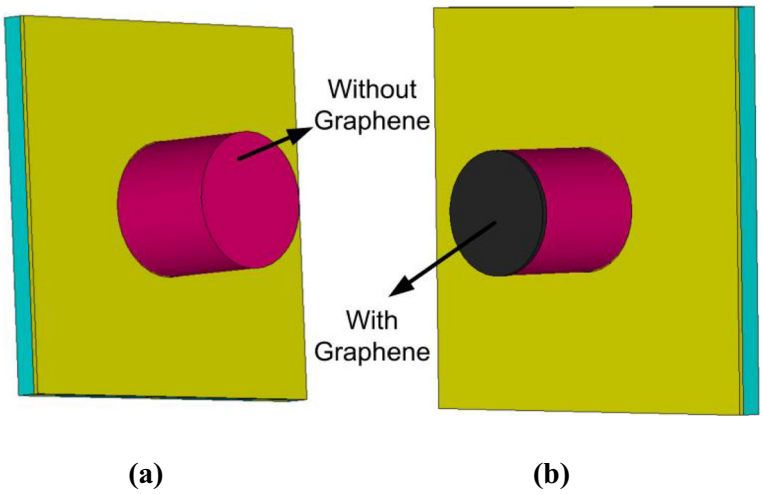

Fig. 21 CDRA **a** without and **b** with Graphene material

4 CPDRA Response to Graphene

The upper surface of CDRA is coated with graphene. The direct fabrication of graphene films on silicon/silica substrate is developed via a tri-constituent self-assembly route using the procedure given in [42]. Metal-free, ambient-pressure chemical vapour deposition was used to successfully manufacture graphene on single-crystal silicon substrates. Controlling the growth temperature allows for the creation of atomically flat monolayer or bilayer graphene domains, concave bilayer graphene domains, and bulging few-layer graphene domains [43].

The main advantage of using graphene at THz frequency region is its tunability characteristics by varying its chemical potential. According to Kubo formula [44], the surface conductivity of graphene can be given by

$$\sigma(\omega,\mu_c,\Gamma,T)=\frac{je^2(w-j2\Gamma)}{\pi h^2}\left[\frac{1}{(\omega-j2\Gamma)^2}\int_0^\infty \epsilon\left(\frac{\partial\left(f_d(\epsilon)\right)}{\partial\epsilon}-\frac{\partial\left(f_d(-\epsilon)\right)}{\partial\epsilon}\right)d\varepsilon-\int_0^\infty\left(\frac{f_d(-\epsilon)-f_d(\epsilon)}{(\omega-j2\Gamma)^2-4(\epsilon/h)^2}\right)d\varepsilon\right] \quad (2)$$

Equation (2) is the sum of intra band (1st term) and inter band (2nd term) conductivity contributions. Where e is electron charge, h is the Planck's constant, $f_d(\epsilon)=\left(e^{(\varepsilon-\mu_c)}/k_B\,T+1\right)^{-1}$ is the Fermi-Dirac distribution, K_B is the Boltzmann's constant. Γ is the chemical potential, ω is the radian frequency, and T = 300 K. A relationship between voltage and μ_c is depicted in eq. (2) depending on the external DC bias voltage applied. According to [45], the relation between DC bias, μ_c depends on the applied voltage V by using Eq. 3.

$$V=V_0+\frac{te\mu_c^2}{\varepsilon_0\varepsilon_r\pi h^2 v_F^2} \quad (3)$$

Where $v_f = 9.5 \times 10^5$ m/s is the fermi level velocity, V_0 is the voltage compensation dependent on the chemical doping, t and ε_r are the height and relative permittivity of the dielectric between graphene and electrode respectively.

The conductivity of graphene can be varied by providing an electric field via DC bias. As stated in [46], the electric field changes the charge density. Equation (4) gives the relationship between electrostatic bias and chemical potential. Figure 20 depicts the relationship between the biasing voltage with chemical potential and relative permittivity of graphene. A metallic gate layer is placed at the top of the graphene patch to apply the DC gate voltage in the antenna configuration. When the external voltage is applied, the length and

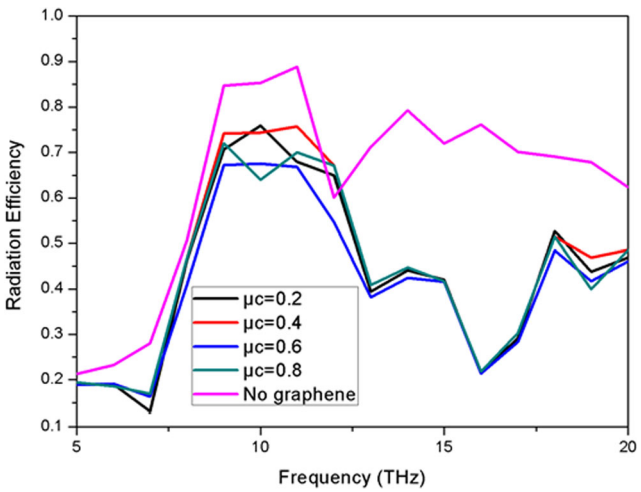

Fig. 22 CDRA Radiation efficiency for different values of Graphene chemical potential

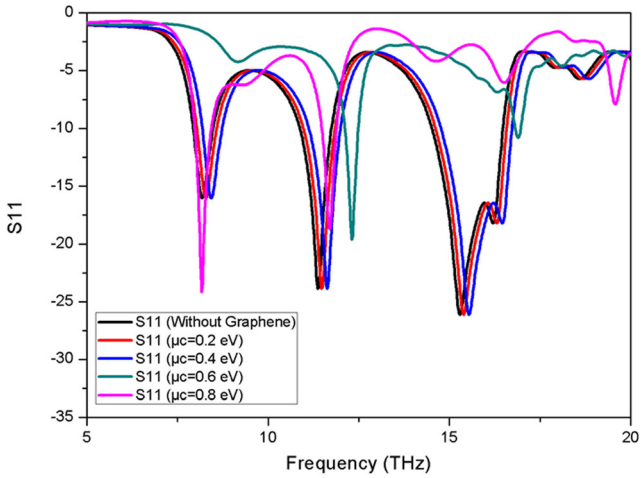

Fig. 23 CDRA frequency response (S_{11}) for different values of Graphene chemical potential

width of the metallic gate layer are kept identical to the graphene patch so that the fermi level is maintained uniformly [47].

$$\frac{2\epsilon_s E_0}{e} = \frac{2}{\pi h^2 v_f^2}\int_0^\infty E(f_d(E) - f_d(E + 2\mu_c))dE \quad (4)$$

Figure 21 shows the structure of CDRA with and without graphene. The radiation efficiency of the CDRA with and without graphene material is depicted in Fig. 22 for different values of chemical potential (μ_c) of graphene. The graphene material having thickness 0.34 nm and T = 300 K is chosen. It is observed that the antenna without graphene provides maximum gain of 85% efficiency whereas 70% gain is shown by the antenna coated with graphene. The main disadvantage of using graphene is there will be reduce in radiation efficiency of the antenna. It is observed that there is linear decrease in efficiency of antenna with increase in μc. Fig. 23 shows the frequency response (S_{11}) with and without graphene. Results shows there is forward shift in the resonant frequency of the antenna for change in μc from 0.2 eV to 0.8 eV.

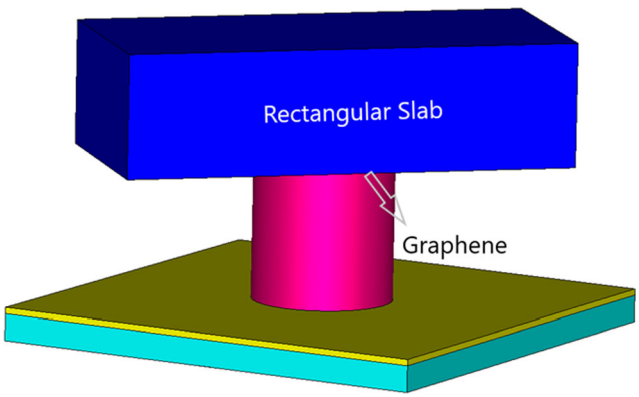

Fig. 24 Structure of proposed CPDRA with graphene

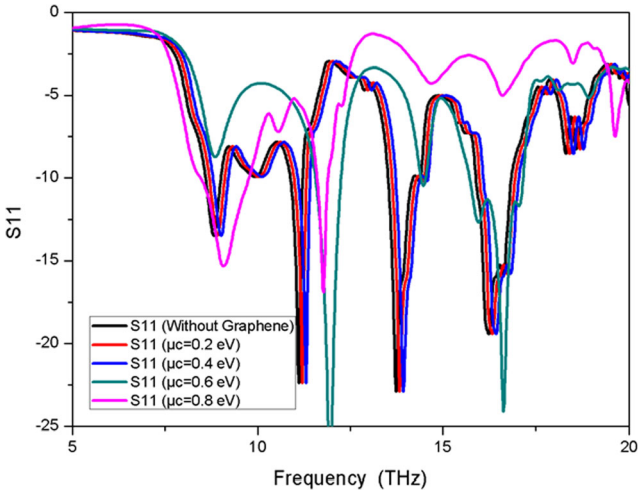

Fig. 25 CPDRA frequency response (S_{11}) with graphene and without graphene material

The tunability property of graphene material can be used to tune the antenna response after it has been manufactured. The external electrostatic DC voltage can be used to change the chemical potential and consequently the conductivity of graphene material. As previously stated, changes in μ_c modify the conductivity of graphene and hence the antenna's operating frequency. The structure of Rectangular slab with CDRA layered with graphene is depicted in Fig. 24. Observations are made in terms of S_{11}, RE, AR and gain of the antenna.

Figure 25 shows the frequency response (S_{11} in dB). Consequently, antenna coated with graphene has its tunability characteristics. There is a forward shift in the resonant frequency of the antenna for varying graphene potential (μ_c). For graphene with μ_c=0.2eV, it resonates at f= 8.854, 11.337, 14.004 and 16.412 THz. For graphene with μ_c=0.4eV is resonates at f=8.91, 11.46 THz. For graphene with μ_c=0.6eV, it resonates at f= 9.50, 11.92 and 16.89. For graphene with μc=0.8eV, it resonates at f= 9.89, 12.97 and 16.98. The findings of RE for different graphene

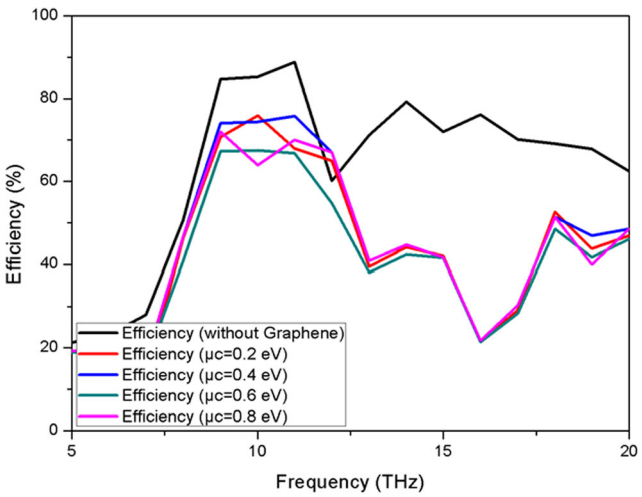

Fig. 26 RE for different values of Graphene chemical potential for CDRA incorporated with Rectangular slab

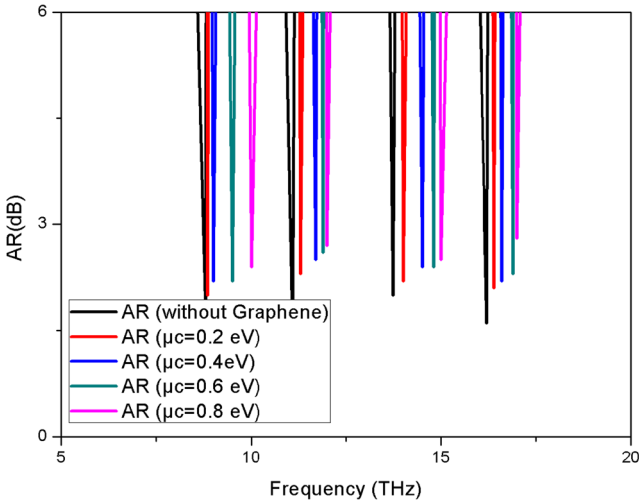

Fig. 27 AR (dB) for different values of Graphene chemical potential

chemical potential values is examined. Figure 26 shows RE for different values of Graphene chemical potential (μ_c= 0.2, 0.4, 0.6, 0.8 eV) for the proposed antenna. Typically, RE with graphene coated antenna provides less efficiency compared to without graphene. 89% RE is achieved for antenna without graphene whereas, a maximum of 78% RE is achieved with graphene. Moreover graphene with 0.8ev provides less RE compared to other potential values.

The axial ratio for different values of graphene potential for the antenna is compared with the antenna without graphene material. Apparently, results shows that AR is less than 3 dB in the pass-band as shown in the Fig. 27. Hence it is clear that antenna with different values of μc achieves quad band CP tuning which is unique feature at THz frequency region. Figure 28 shows the plot between gain of the antenna (dB) with frequency (THz). CDRA with graphene provides maximum gain of 5.8 dB. Whereas for the antenna without graphene a maximum gain of 6.5 dB is achieved. Finally, an Rectangular slab on top of CDRA with and without graphene is designed and performance analysis is

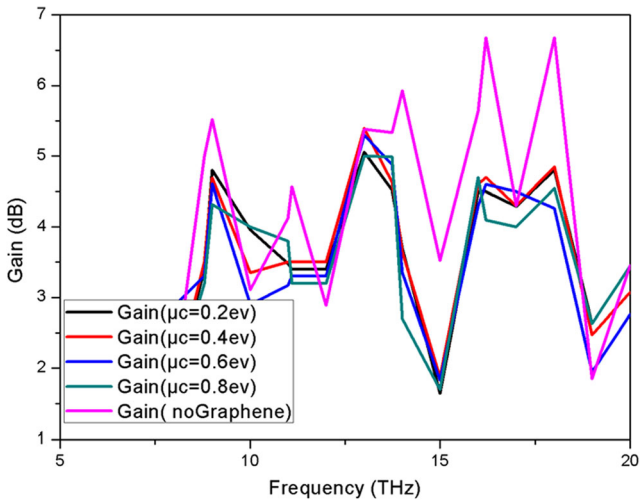

Fig. 28 Frequency vs Gain for different graphene potential values

Table 2 Comparison with other antennas

Ref	Antenna	ARBW(THz)	IBW(THz)	Gain(dB)	RE (%)	Tunability
[34]	Graphene based microstrip antenna	–		1.6		No
[35]	Slotted graphene patch antenna	–	1.96 THz (Center Frequency)	4.3	95.3	No
[36]	Y-shaped graphene-based antenna	–	0.45THz (Center Frequency)	4	25%	No
[37]	Patch Fed Higher Order Mode DRA		7%	7.9	–	No
[27]	CPDRA	3.97–4.16	3.95–4.1	>6	>80%	Yes
[39]	Graphene disk loaded DR	–	4.0629–4.1299	3.8	72–75%	Yes
This antenna	Quad band Rectangular slab incorporated CDRA based Circularly polarized tunable THz antenna	1.83% (8.66–8.82 THz), 6.64% (10.77–11.51), 3.84% (13.26–13.78 THz) and 4.8% (16.04–16.83 THz)	4.66% (8.59-9THz), 2.98% (10.88–11.21THz), 4.83% (14.19–13.52THz) and 5.86%(15.88–16.84)	>6	>85%	Yes

being carried out. It can be concluded that addition of graphene adds tunability to the proposed antenna and will not affect Quad Band CP behavior of the antenna. Additionally antenna with graphene provides good gain and efficiency in the targeted pass bands. According to the desired frequency of operation, the antenna can be manufactured with the optimal values of its physical parameters.

Table 2 shows the comparison of proposed antenna with other antennas. This proposed antenna provides CP behavior at quad band in the field of THz dielectric resonator antennas and also CP tuning is achieved by varying graphene potential of the antenna.

5 Conclusion

A CDRA along with Rectangular DR slab known as CPDRA with graphene coating is implemented for terahertz (THz) applications. This antenna provides multi-mode response at different resonant frequencies. An IBW of 6.7% (7.93–8.48 THz), 7.6% (11.74–10.87 THz) and 12.65% (14.51–16.47 THz) is attained for CDRA. Unique feature of the proposed CPDRA antenna is, it provides CP behaviour at quad band in the field of THz dielectric resonator antennas and also CP tuning is achieved by varying graphene potential of the antenna. This proposed antenna shows both RHCP and LHCP behaviour at different resonant frequencies. Furthermore, in the THz frequencies, the designed antenna has a high gain and high radiation efficiency (RE). Results shows that a maximum gain of 6.67 dB, RE of 89%, Impedance Band Width of 4.66% (8.59-9THz), 2.98% (10.88–11.21THz), 4.83% (14.19–13.52THz) and 5.86%(15.88–16.84), Axial Ratio Bandwidth of 1.83% (8.66–8.82 THz), 2.16% (10.94–11.18), 3.84% (13.26–13.78 THz) and 4.8% (16.04–16.83 THz) is achieved by the combination of CDRA and Rectangular slab. Graphene material is added to the top of CDRA to achieve tunability in CP response. All these results show the proposed Quad band CPDRA is unique and suitable for THz applications.

Authors' Contributions All authors contributed to the study conception and design. Material preparation, data collection and analysis were performed by all the authors. The first draft of the manuscript was written by P. UPENDER and all authors commented on previous versions of the manuscript. All authors read and approved the final manuscript.

Funding The authors have no financial or proprietary interests in any material discussed in this article.

Data Availability Not applicable.

Declarations

Ethics Approval and Consent to Participate Not applicable.

Disclosure of Potential Conflicts of Interest Not applicable.

Research Involving Human Participants and/or Animals Not applicable.

Informed Consent Not applicable.

Consent for Publication The manuscript is entitled "Quad-band Circularly Polarized Tunable graphene based Dielectric Resonator Antenna for Terahertz Applications". It has not been published elsewhere and that it has not been submitted simultaneously for publication elsewhere.

Competing Interests The authors have no relevant financial or non-financial interests to disclose.

References

1. Long SA, Mcallister MW, Shen LC (1983) The resonant cylindrical dielectric cavity antenna. IEEE Trans Antennas Propag 31(3):406–412. https://doi.org/10.1109/TAP.1983.1143080
2. Milligan TA (2005) Modern antenna design2nd edn. Wiley, New Jersey
3. Balanis CA (2005) Antenna theory: analysis and design3rd edn. John Wiley
4. Petosa A, Ittipiboon A (Oct. 2010) Dielectric resonator antennas: a historical review and the current state of the art. IEEE Antennas Propag Mag 52(5):91–116
5. Leung KW, Lim EH, Fang XS (2012) Dielectric resonator antennas: from the basic to the aesthetic. Proc IEEE 100(7):2181–2193
6. Wen J, Jiao YC, Zhang YX, Jia J (2019) Wideband circularly polarized dielectric resonator antenna loaded with partially reflective surface. International Journal of RF and Microwave Computer-Aided Engineering 29(12)
7. Nawaz H, Shahid S, Gentili G (2015) Wideband dielectric resonator antenna using CPW fed segments. Microw Opt Technol Lett 58(2):441–445
8. Kong S, Shum KM, Yang C, Gao L, Chan CH (2021) Wide Impedance-and Gain-Bandwidth Terahertz On-Chip Antenna with Chip-Integrated Dielectric Resonator. IEEE Trans Antennas Propag. https://doi.org/10.1109/TAP.2021.3060060
9. Zhang M, Li B, Lv X (2014) Cross-slot-coupled wide dual-band circularly polarized rectangular dielectric resonator antenna. IEEE Antennas Wirel Propag Lett 13:532–535. https://doi.org/10.1109/LAWP.2014.2310241
10. Fumeaux C et al (2016) Terahertz and optical dielectric resonator antennas: potential and challenges for efficient designs. 2016 10th European conference on antennas and propagation (EuCAP), Davos, Switzerland, pp 1–4. https://doi.org/10.1109/EuCAP.2016.7481118
11. Xia W, Zhang B, Zhou W, Zhang J, Liu C, He D, Wu Z (2021) Rectangular dielectric resonator antenna fed by offset tapered copper and graphene microstrip lines for 5G communications, April-2021
12. Md. Muzammil Sani, Rakesh Chowdhury, Raghvendra Kumar Chaudhary (2021) Design and analysis of multiple input multiple output antenna for wideband applications using cylindrical dielectric resonator, AEU - International Journal of Electronics and Communications, Volume 131
13. Chauhan M, Rajput A, Mukherjee B (2021) Wideband circularly polarized low profile dielectric resonator antenna with meta superstrate for high gain. AEU Int J Electron Commun 128

14. Okan T (2021) High efficiency Unslotted ultra-wideband microstrip antenna for sub-terahertz short range wireless communication systems. Optik 242:166859
15. Shalini M, Ganesh MM (2021) A compact antenna structure for circular polarized terahertz radiation. Optik 231
16. Li S, Zhang X (2019) An ultra-wideband linear to circular polarization converter in reflection mode at terahertz frequencies. Microw Opt Technol Lett 61(12):2675–2680
17. Dash S, Patnaik A (2018) Material selection for THz antennas. Microw Opt Technol Lett 60(5):1183–1187
18. Singh RK, Gupta A (2021) A wrenched-square shaped polarization independent and wide angle stable ultra-thin metamaterial absorber for S-band, X-band and Ku-band applications. AEU Int J Electron Commun 132
19. Chen XF, Zhao YJ (2018) Dual-band polarization and frequency reconfigurable antenna using double layer metasurface. AEU Int J Electron Commun 95:82–87
20. Chen Z, Wong H, Kelly J (2019) A polarization-reconfigurable glass dielectric resonator antenna using liquid metal. IEEE Trans Antennas Propag 67(5):3427–3432. https://doi.org/10.1109/TAP.2019.2901132
21. Ren X, Liao S, Xue Q (2019) A circularly polarized Spaceborne antenna with shaped beam for earth coverage applications. IEEE Trans Antennas Propag 67(4):2235–2242. https://doi.org/10.1109/TAP.2018.2889188
22. Guo Q-Y, Lin QW, Wong H (2021) A high gain millimeter-wave circularly polarized Fabry–Pérot antenna using PRS-integrated polarizer. IEEE Trans Antennas Propag 69(2):1179–1183. https://doi.org/10.1109/TAP.2020.3011110
23. Guo Q-Y, Wong H (2021) 155 GHz dual-polarized Fabry–Perot cavity antenna using LTCC-based feeding source and phase-shifting surface. IEEE Trans Antennas Propag 69(4):2347–2352. https://doi.org/10.1109/TAP.2020.3019528
24. Yang N, Leung KW (2020) Compact cylindrical pattern-diversity dielectric resonator antenna. Antennas Wirel Propag Lett 19(1):19–23. https://doi.org/10.1109/LAWP.2019.2951633
25. Sharma A, Das G, Gupta S, Gangwar RK (2020) Quad-band quad-sense circularly polarized dielectric resonator antenna for GPS/CNSS/WLAN/WiMAX applications. IEEE Antennas Wirel Propag Lett 19(3):403–407. https://doi.org/10.1109/LAWP.2020.2969743
26. Gupta R, Varshney G, Yaduvanshi RS (2021) Tunable terahertz circularly polarized dielectric resonator antenna. Optik 239
27. Varshney G, Debnath S, Sharma AK (2020) Tunable circularly polarized graphene antenna for THz applications. Optik 223
28. Sa'don SNH, Jamaluddin MH, Kamarudin MR, Ahmad F, Yamada Y, Kamardin K, Idris IH, Seman N (2020) Characterisation of tunable graphene antenna. AEU Int J Electron Commun 118:153170
29. Hosseininejad SE et al (2018) Terahertz dielectric resonator antenna coupled to graphene plasmonic dipole. 12th European conference on antennas and propagation (EuCAP 2018), London, UK, pp 1–5, doi: https://doi.org/10.1049/cp.2018.1041
30. Varshney G, Singh R, Pandey VS, Yaduvanshi RS (2020) Circularly polarized Two-port MIMO dielectric resonator antenna, Progress In Electromagnetics Research
31. Li X, Yin W, Khamas S (2020) An Efficient Photomixer Based Slot Fed Terahertz Dielectric Resonator Antenna. 2020 International workshop on antenna technology (iWAT), Bucharest, Romania, pp 1–4. https://doi.org/10.1109/iWAT48004.2020.1570618183
32. H. Nawaz and M. Ali Babar Abbasi, "Wide-band dielectric resonator antenna using K-shaped fractal," Microw Opt Technol Lett, vol. 58, no. 6, pp. 1504–1507, 2016
33. Nissiyah GJ, Madhan MG (2021) Graphene based microstrip antenna for triple and quad band operation at terahertz frequencies. Optik 231:1663606
34. Shalini M, Ganesh Madhan M (2020) Performance predictions of slotted graphene patch antenna for multi-band operation in terahertz regime. Optik 204:164223
35. Chashmi MJ, Rezaei P, Kiani N (2020) Y-shaped graphene-based antenna with switchable circular polarization. Optik 200
36. Li C, Chiu T (2017) 340-GHz low-cost and high-gain on-chip higher order mode dielectric resonator antenna for THz applications. IEEE Trans Terahertz Sci Technol 7(3):284–294. https://doi.org/10.1109/TTHZ.2017.2670234
37. Varshney G (2021) Tunable terahertz dielectric resonator antenna. Silicon 13:1907–1915
38. Novin SN, Zarrabi FB, Bazgir M, Heydari S, Ebrahimi S (2019) Field enhancement in metamaterial split ring resonator aperture nano-antenna with spherical nano-particle arrangement. Silicon 11:293–300
39. Nourmohammadi A, Nikoufard M (2020) Ultra-wideband photonic hybrid plasmonic horn nanoantenna with SOI configuration. Silicon 12:193–198
40. Huitema L, Monediere T (2012) Dielectric materials for compact dielectric resonator antenna applications. Dielectric Material
41. Luk KM, Leung KW (eds) (2003) Dielectric resonant antenna. Research Studies Press
42. Yang Y, Liu R, Wu J, Jiang X, Cao P, Hu X, Pan T, Qiu C, Yang J, Song Y, Wu D, Su Y (2015) Bottom-up fabrication of graphene on silicon/silica substrate via a facile soft-hard template approach. Sci Rep 5:13480
43. Tai L, Zhu D, Liu X, Yang T, Wang L, Wang R, Jiang S, Chen Z, Xu Z, Li X (2018) Direct growth of graphene on silicon by metal-free chemical vapor deposition. Nano-Micro Lett 10:20. https://doi.org/10.1007/s40820-017-0173-1
44. Chen P, Argyropoulos C, Alù A (2013) Terahertz antenna phase shifters using integrally-gated graphene transmission-lines. IEEE Trans Antennas Propag 61(4):1528–1537. https://doi.org/10.1109/TAP.2012.2220327
45. Liang F, Yang Z, Xie Y, Li H, Zhao D, Wang B (2018) Beam-scanning microstrip Quasi-Yagi–Uda antenna based on hybrid metal-graphene materials. IEEE Photon Technol Lett 30(12):1127–1130. https://doi.org/10.1109/LPT.2018.2835840
46. Hanson GW (2008) Dyadic Green's functions for an anisotropic, non-local model of biased graphene. IEEE Trans Antennas Propag 56(3):747–757. https://doi.org/10.1109/TAP.2008.917005
47. Varshney G, Gotra S, Pandey VS, Yaduvanshi RS (2019) Proximity-coupled two-port multi-input-multi-output graphene antenna with pattern diversity for THz applications. Nano Commun Netw 21:100246. https://doi.org/10.1016/j.nancom.2019.05.003